Assessing the Reliability and Degradation of Photovoltaic Module Performance Parameters

Edson L. Meyer and E. Ernest van Dyk

***Abstract*—Photovoltaic (PV) modules are renowned for their reliability. However, some modules degrade or even fail when operating outdoors for extended periods. To reduce the degradation, and the number of failures, extensive research is needed on the performance of PV modules. The aim of this study was to establish a photovoltaic degradation and failure assessment procedure. This procedure should assess all parameters of PV modules to completely analyze any observed degradation or failure.**

In this paper some degradation modes of PV modules are discussed and a procedure used to assess these degradation modes is then presented. Results obtained by subjecting Copper Indium Diselenide (CIS), single and triple junction amorphous silicon (a-Si and a-SiGe), Edge-defined Film-fed Growth (EFG) silicon and mono-crystalline silicon (mono-Si) modules to the assessment procedure are presented and discussed. Results obtained indicate that the thin-film modules degrade by up to 50% in performance after an initial outdoor exposure of 130 $\mathrm{kWh/m^2}$. Visual inspection revealed that both crystalline modules had cracked cells. The mismatch due to the cracked cell in the EFG-Si module, however, was limited by the interconnect busbars. This paper accentuates the importance of characterizing all module performance parameters in order to analyze observed degradation and failure modes.

***Index Terms*—Assessment procedure, degradation analysis, degradation and failure modes, improving reliability, performance parameters, photovoltaic module.**

ACRONYMS[1]

AR	anti-reflective
CIS	copper indium diselenide (CuInSe2)
DAS	data acquisition system
EVA	ethylene vinyl acetate
FF	Fill Factor
HPVEE	Hewlett Packard visual engineering environment
POA	plane-of-array
PV	photovoltaic
PVSIM	photovoltaic simulation program
STC	standard test conditions, 1000 $\mathrm{W/m^2}$, 25°C cell temperature, and Air Mass 1.5 global spectrum
UV	ultraviolet

NOTATION

$\mathrm{I_{01}}$,$\mathrm{I_{02}}$	the reverse saturation currents of the two diodes
k	the Boltzmann constant $= 1.38 \times 10^{-23}$ J/K
$\mathrm{n_1}$, $\mathrm{n_2}$	the diode ideality factors and $\mathrm{n_1}$ is assumed to be unity
q	the elementary charge
$\mathrm{R_s}$	the cell's series resistance
$\mathrm{R_{sh}}$	the shunt resistance
T	the absolute cell temperature
$\mathrm{V_i}$	$\mathrm{V - IR_s}$
V	the applied voltage across the p-n junction solar cell

Manuscript received December 10, 2001; revised April 29, 2002. Responsible Editor: R. M. Burger. This work was supported by the NRF, ESKOM and the UPE Research Committee.

E. L. Meyer is with the Department of Physics, University of Fort Hare, Alice, 5700, South Africa (e-mail: emeyer@ufh.ac.za).

E. E. van Dyk is with the University of Port Elizabeth, Port Elizabeth, 6000, South Africa (e-mail: Ernest.vanDyk@upe.ac.za).

Digital Object Identifier 10.1109/TR.2004.824831

[1]The singular and plural of an acronym are always spelled the same.

I. INTRODUCTION

ALTHOUGH photovoltaic (PV) modules are a very reliable source of electrical energy, field results [1], [2] indicate that the modules can fail or degrade in a number of ways. Before trying to eliminate or even reduce these degradation modes, a thorough understanding of their origin and behavior is required. In this study, degradation modes are analyzed by measuring various PV module performance parameters before the modules are deployed outdoors and regularly thereafter. Understanding the origin of these degradation modes and how they affect the performance of PV modules is essential to improve the reliability of PV modules. This is especially true for the relatively low cost thin-film modules, which are known to degrade when first exposed to light. Once the effect of these modes on all performance parameters is known, researchers can then devise ways to limit or even eliminate the degradation. Section II deals with some degradation modes observed in PV cells and modules, as well as their origin and effect on PV module performance parameters. Section III then presents the assessment procedure used to analyze these degradation modes. The five modules used in this study were initially subjected to the assessment procedure and then deployed outdoors. The assessment procedure was then repeated during and after an irradiation of 130 $\mathrm{kWh/m^2}$. Results obtained are used to analyze the degradation in the thin film module performance and the effect of cell imperfections on module performance.

II. DEGRADATION MODES

A. Front Surface Soiling

This degradation mode can occur due to the accumulation of dirt on the module's top surface. These losses are kept below 10% for glass-surfaced modules due to self-cleaning by wind and rain. The accumulated dirt may, however, partially shade a cell in the module causing it to produce less current than the other string cells. If there is insufficient electrical protection, the partial shading of the cell can lead to irreversible hot-spot damage and even module failure [3]. Front surface soiling can be detected by visual inspection of the module and in-field inspection.

B. Optical Degradation

Optical degradation may result from discoloration of the encapsulating material. Due to ultraviolet (UV) exposure, temperature, or humidity, yellowing of the encapsulating material can occur after extended exposure periods. It can also occur due to the diffusion of dirt from the front surface soiling and moisture ingress from the edge seals.

When Ethylene Vinyl Acetate (EVA) is used as an encapsulant, its lifetime may be increased by using UV stabilizers and anti-oxidants. The stabilizer concentration, however, decreases gradually at elevated temperatures and when exposed to UV irradiation [4]. When this stabilizer concentration drops below some critical value, rapid degradation of the encapsulant occurs. This degradation is associated with the yellowing of the EVA, which is accompanied by the formation of acetic acid. The latter causes the EVA to turn brown. The brown EVA absorbs a significant fraction of sunlight in the UV and visible region thereby reducing the photon availability required for current generation. This browning of the encapsulant can decrease the module performance by as much as 50% [5]. The degradation of the EVA can be visually detected by illuminating the module with a 375-nm ultraviolet lamp. Under these conditions, regions of the EVA that have started to degrade will produce a nearly white color [6].

C. Cell Degradation

Solar cell degradation can be caused by three factors resulting in a gradual degradation in module performance. These factors are an increase in the cell's series resistance, $\mathrm{R_s}$; a decrease in the cell's shunt resistance, $\mathrm{R_{sh}}$; and an antireflection coating deterioration. Fig. 1 shows the two-diode equivalent-circuit model of a solar cell, illustrating the series and shunt resistances. These cell specific degradation modes are important factors in analyzing PV cell and module degradation and failures. These modes can gradually degrade module performance over extended operational periods and are discussed below.

1) Series Resistance: The series resistance, $\mathrm{R_s}$, of a PV module arises from resistances in cell solder bonds, emitter and base regions, cell metallization, cell-interconnect busbars and resistances in junction-box terminations [7]. The series resistance reduces the voltage produced by the cell, which ultimately reduces the performance of the PV cell, and hence the module. Although cell and module designers minimize series resistance losses, daily thermal cycling of modules deployed outdoors results in a gradual increase in series resistance. Dark current-voltage (I-V) measurements can be used to quantitatively evaluate increases in series resistances. These measurements are also sensitive to changes in module shunt resistance and other cell parameters [8], [9].

2) Shunt Resistance: The shunt resistance, $\mathrm{R_{sh}}$, represents any parallel high-conductivity paths (shunts) through the solar cell or on the cell edges [10]. These would be due to crystal damage and impurities in and near the junction, and give rise to the shunt current, $\mathrm{I_{sh}}$, shown in Fig. 1. These shunt paths lead currents away from the intended load and their effects are detrimental to the module performance especially at low intensity levels. The number of shunts in thin-film cells may increase after prolonged exposure to light [10]. The increase in the number of shunts increases the effective shunt current in the cell, and hence decreases $\mathrm{R_{sh}}$. A nonintrusive two terminal method [10], [11] can be used to measure the individual cell shunt resistance in a module.

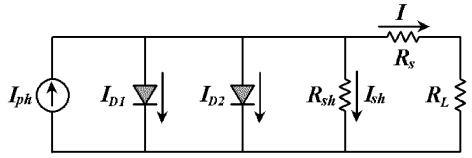

Fig. 1. Equivalent-circuit model of a solar cell. $\mathrm{I_{ph}}$ is the photogenerated current, ID the dark recombination current, $\mathrm{R_{sh}}$ the shunt resistance, $\mathrm{R_s}$ the series resistance and $\mathrm{R_L}$ the load.

3) Anti-Reflective Coating: The reflectivity of bare silicon is about 35% at the maximum intensity of the solar spectrum, which occurs at a wavelength of 600 nm [12]. This percentage can be reduced to around 20% by texturing the surface and to about 3% by adding an anti-reflective (AR) coating [13]. A low reflectivity improves both short-circuit current and open-circuit voltage, which in turn enhances the conversion efficiency of a PV cell [12]. AR coatings must for obvious reasons be transparent and are, therefore, usually oxides. The degradation of these coatings after time may be attributed to inter-diffusion of species from the cell's emitter region to the AR coating and vice versa. The effect of the degradation of the AR coating of a cell in a series connected string, is that the cell will now absorb less incoming photons and hence produce less current than the other string cells. The result is a mismatched cell, which is discussed in the next section. Degradation of AR coatings is observed as a brightening in the color of the cell. It can also be detected by monitoring the module's short-circuit current and open-circuit voltage over time [14].

D. Mismatched Cells

Mismatched cells are caused by front surface soiling, encapsulant degradation, AR coating deterioration, manufacturing defects, cell cracking, and partial shading of the PV cell. Mismatched cells degrade module performance and are detrimental, especially when the cells are all connected in series strings in a module.

When a cell in a module is producing less current than the other module cells, the latter cells act to reverse bias the former, defective cell. This causes the defective cell to operate in the negative voltage region where it becomes a power dissipater [15]. Fig. 2(a) shows how interconnect busbars can help prevent a cell from producing less current due to the illustrated crack. Thermal stress, and hail damage can cause cracking of cells. Cracks can also be formed during processing and assembly. The crack in Fig. 2(b) removes a part of the cell from its electrical circuit. This will have the effect of a reduced current produced by the cell. The same phenomenon is observed when a cell is partially shaded.

Mismatched conditions in solar cells cause the cells to heat up. When the mismatched cell's temperature exceeds a critical value ($\sim 150°$), delamination of cell encapsulants may occur [15]. If the high reverse bias exceeds the cell's breakdown voltage, the cell may be irreversibly damaged by thermal breakdown. The latter is observed as the formation of hot spots on the cell. Hot-spot formation in solar cells and modules not only lowers the efficiency of the module, but also influences the open-circuit

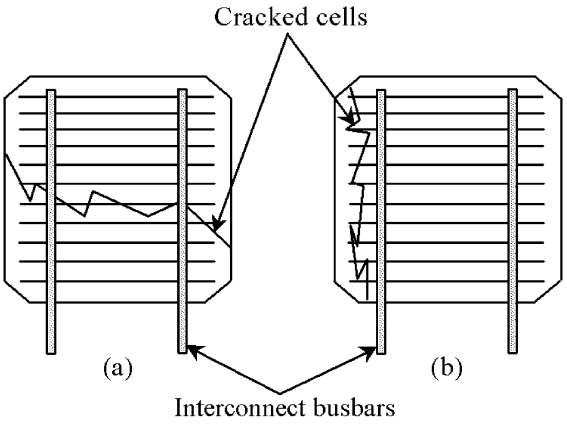

Fig. 2. Illustration of how interconnect busbars can help prevent open-circuit failure.

voltage (V_{oc}), the short circuit current (I_{sc}), the maximum power (P_{max}), and the fill factor ($FF = P_{max}/I_{sc}V_{oc}$). If a module containing a mismatched cell has no integrated bypass diode in its interconnection circuit, a mismatch situation may lead to irreversible hot spot damage. Mismatched cells can usually be detected by visual inspection, I-V measurements, hot-spot endurance testing and/or individual cell temperature monitoring when the module is forward biased.

E. Light-Induced Degradation

Also referred to as the Staebler-Wronski effect [16], light-induced degradation is the dominant degradation mode in a-Si and a-Si alloys. When PV cells are exposed to light, generation and recombination of electron-hole (e-h) pairs occurs. It is believed that the energy released during recombination may break some of the weak Si-Si bonds in the cell's depletion region. These broken bonds form meta-stable defects, which in turn act as recombination centers. These centers enhance recombination of e-h pairs and, hence, the formation of more meta-stable defects. The increase in defects deteriorates the quality of the material. This lower quality is consequently translated to degradation in the solar cell performance [17]. Light-induced degradation can be detected by continuously monitoring I_{sc} and V_{oc} and/or by periodic measurement of I-V characteristics [14].

F. Temperature-Induced Degradation

PV modules are rated by their power as measured at standard test conditions (STC: 1000 W/m^2 irradiance, 25°C cell temperature and Air Mass 1.5 global spectrum). However, when a module is operating outdoors, only about 15% of the incident energy is converted to electricity. A large fraction of the remaining 85% is transformed into heat while the rest may be internally reflected or reflected at the glass surface. It is therefore obvious that a module, operating outdoors, will almost always have a temperature above 25°C. At these elevated temperatures, the bandgap of the cells usually decreases, implying that longer wavelength photons can now be absorbed. Also, as temperature increases, the minority carrier lifetime generally increases. Both these factors will slightly increase the light generated current and consequently I_{sc}. The saturation current, however, decreases exponentially with increase in temperature [18]. This acts to reduce the cell's V_{oc} as temperature increases. The decrease in V_{oc} is more rapid than the increase in I_{sc}, resulting in an overall reduction in the cell's fill factor, and hence, efficiency as the temperature increases.

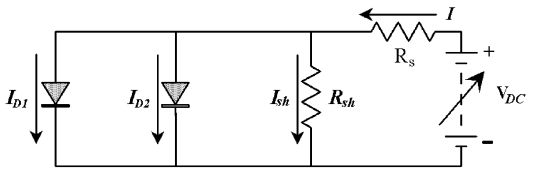

Fig. 3. Two-diode equivalent solar cell circuit for a cell in the dark.

Elevated temperatures influence the performance of all modules, some more than others. For this reason, it is important to know the temperature dependence of each module. By measuring the temperature dependence of the modules, a change in the temperature coefficient can be detected. These coefficients can also be used to explain the behavior of the modules when operating outdoors.

III. Degradation Analysis

To analyze the degradation of photovoltaic modules, a complete set of evaluation methods is necessary. This procedure should be conducted on modules before they are subjected to outdoor operating conditions and on a regular basis while the modules are deployed outdoors. An assessment procedure established at the University of Port Elizabeth, South Africa is used to evaluate PV modules. The procedure is presented below.

A. Comprehensive Visual Inspection

Modules are thoroughly inspected for visual defects under low magnification. Photographs are taken from observed defects so as to ensure that these defects are positively identified for future reference. The visual inspection will reveal defects such as cracked or partially shaded cells, interconnect imperfections, "browning" of the encapsulant, and the formation of hot spots.

B. Light I-V Measurement

The I-V characteristics of PV modules are measured at STC before outdoor deployment and used as a baseline for future comparison. These measurements are done using a SPIRE SUN simulator 240 employing an electronic load to generate the I-V characteristics. I-V characteristics can also be used to establish if a module contains a defective cell. These characteristics are essential to detect any degradation of the module performance parameters as the measurement is repeated at regular intervals. The I-V characteristics are also measured regularly outdoors using an array tester. Parameters like I_{sc}, V_{oc}, P_{max} and FF are obtained from I-V measurements. The FF is a measure of the junction quality and the series resistance, R_s, of a cell [7].

C. Dark I-V Measurement

The dark I-V characteristics of PV modules are measured forward biasing a module in the dark [19]. Although the current direction out of the module is opposite to that of a module operating in the light, the direction of the diode current, I_D, and the shunt current, I_{sh}, is the same for both light and dark I-V measurements. Fig. 3 illustrates R_s, R_{sh}, and I_D in the two-diode equivalent circuit model of a p-n junction solar cell in the dark.

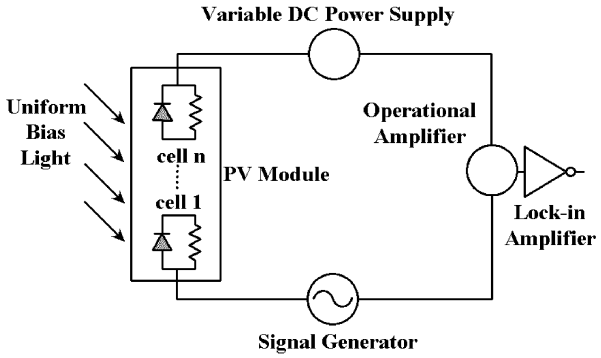

Fig. 4. Schematic representation of the shunt resistance measurement system used to measure individual cell shunt resistance of encapsulated modules.

The dark current-voltage characteristic of the equivalent circuit model is given by [19]:

$$I = I_{D1} + I_{D2} + I_{sh} \quad (1)$$

$$I = I_{01}\left[e^{qVi/n_1kT} - 1\right] + I_{02}\left[e^{qVi/n_2kT} - 1\right] + \frac{V_i}{R_{sh}}. \quad (2)$$

Therefore, cell parameters like R_s, R_{sh}, I_o and n_2 can be obtained by fitting (2) to a set of experimental data. This fit is obtained by nonlinear regression analysis of dark I-V measurement data [9]. If conducted regularly, R_s of a module can be monitored to see if it has increased due to bad contacts resulting from corrosion, for example.

D. Shunt Resistance Measurement

For a good solar cell, the shunt current should be negligibly small because this current detracts from the light-generated current when the cell is illuminated. Low shunt resistance can detract significantly from the cell performance. Ideally, R_{sh} should be infinitely large. This parameter is crucial to PV performance, especially at reduced irradiance levels [20]. For this reason, it is important to know which cell will stop contributing to module output due to a low shunt resistance. In this test, a nonintrusive technique is used to measure the individual cell shunt resistances of encapsulated modules. A schematic of the shunt resistance measurement system is shown in Fig. 4. Using this method regularly, R_{sh} of a cell can be monitored to see if it has decreased due to an increase in the number of shunt paths.

In this method, the module is set at zero DC bias. A small AC signal is then sent through the module, the only path being the shunt paths of the individual cells. The magnitude of the AC signal when the cells are sequentially shaded, is directly proportional to the conductance of the module in the dark, i.e., the shunt current. Thus, by calibrating the system so that a known resistance gives a certain milli-volt output, it is possible to measure the individual cell shunt resistance. This method is similar to the two-terminal diagnostic technique used by researchers at the National Renewable Energy Laboratory (NREL) [10]. In addition, characterization of module efficiency as a function of light intensity can also be an indication of module shunt resistance [11].

E. Hot-Spot Investigation

This test identifies the cell in a module where the worst-case hot spot condition will occur. The worst-case hot spot condition is obtained from light I-V curves and thermal testing. In the latter, liquid crystal sheets (LCS), and thermocouples are used to monitor cell temperature as a current of at least $2 \times I_{sc}$ is sent through the module.

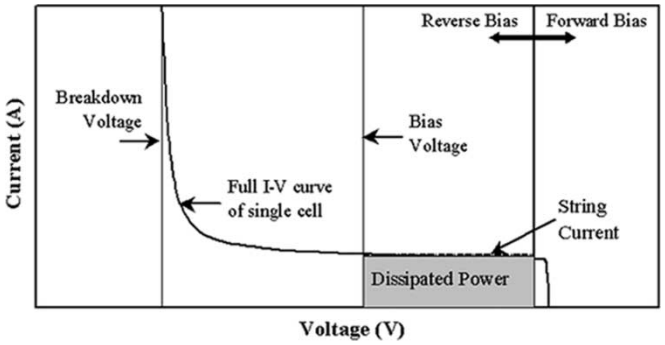

Fig. 5. I-V characteristic of a single PV cell in the forward and reverse directions as generated by PVSIM [22].

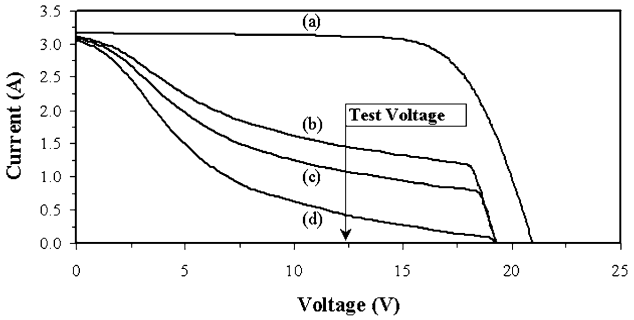

Fig. 6. Determination of the cell in a module where the worst-case hotspot condition will occur. The cell resulting in the highest module current at the test voltage is the worst case cell.

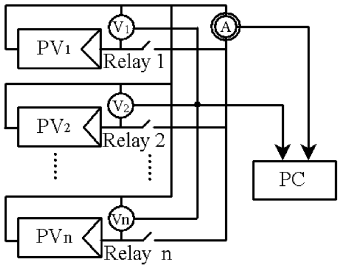

Fig. 7. System design for monitoring module I_{sc} and V_{oc}. All control and measuring devices are interfaced to PC boards.

Fig. 5 shows the light I-V characteristics of a single cell in the forward and reverse voltage range. A PV simulation program, PVSIM [21] was used to generate the I-V characteristics. If this cell is connected in series to other string cells, and producing less current, it becomes reverse biased by the voltage generating capabilities of the other string cells. This causes the defective cell to operate in the negative voltage range where it dissipates power as heat. Thus, the higher the reverse bias, the more power is dissipated and hence, the higher the cell temperature. If the reverse bias exceeds the breakdown voltage of the cell, the cell is irreversibly damaged by, for example, hot spot formation, cell cracking and melting solder.

The worst-case hot spot cell is determined by comparing I-V curves of a module with individual cells sequentially darkened [15]. This method is illustrated in Fig. 6. A test voltage, for example the operating voltage of a typical 12 V stand-alone PV system voltage, can be chosen. All curves were generated using

TABLE I
LIST OF MODULES USED. ALSO LISTED ARE THE MODULES' SPECIFIED AND MEASURED POWERS AND THE APERTURE EFFICIENCIES.

Module	Specified (W)	Measured (W)	η (%)
Copper Indium Diselenide (CIS)	10	10.76	9.19
Single junction amorphous Si (a-Si)	14	12.98	4.41
Triple junction amorphous Si (a-SiGe)	32	34.72	7.69
EFG-Si	32	31.64	11.30
Mono-crystalline Si (mono-Si)	32	29.47	9.07

TABLE II
LIST OF THE ASSESSMENT PROCEDURE.

Test	Objective	Frequency
Visual inspection	Positively identify visual defects	Monthly
I-V measurements (simulator)	Determine electrical characteristics	Monthly
I-V measurements (outdoors)	Determine electrical characteristics	Weekly
Electrical testing	Determine insulation resistance	Monthly
Hot-spot determination	Determine worst-case hot spot condition	Monthly
R_{sh} / Low irradiance measurement	Measure individual cell shunt resistance	Monthly
Dark I-V measurements	Determine R_s, R_{sh}, I_o and ideality factor	Monthly
Temperature dependence	Determine temperature coefficients	Monthly
Monitoring I_{sc} and V_{oc}	Detect any degradation in performance	Continuously

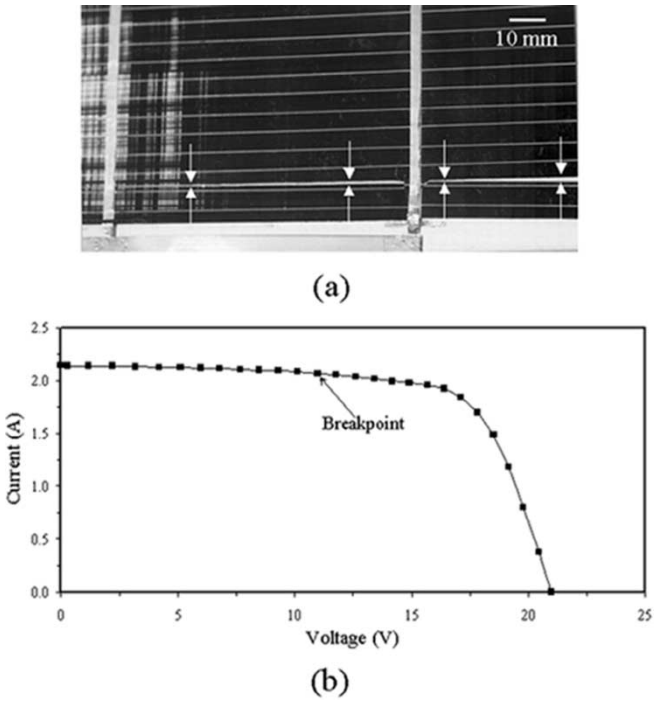

Fig. 8. (a) Cracked cell in the EFG-Si module. (b) The corresponding I-V curve shows a small break in the above 10 V.

PVSIM [21]. Curve (a) of Fig. 6 is the I-V characteristic of a fully illuminated 36-cell PV module. When one cell is fully shaded, the resulting module I-V curve is determined by the reverse I-V characteristic of the shaded cell as shown in curve (b) of Fig. 6. This shaded cell results in the highest module current at the test voltage, which implies that this cell is dissipating

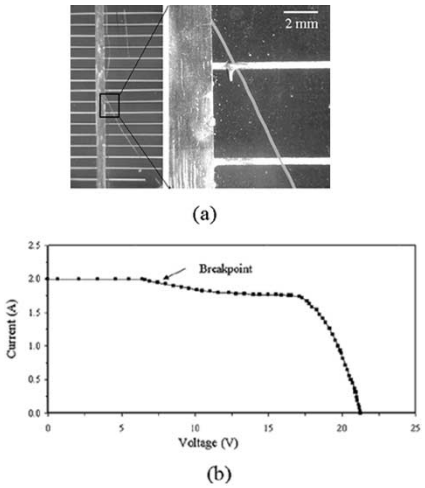

Fig. 9. (a) Cracked cell in the mono-Si module. (b) The corresponding I-V curve shows a break above 5 V.

more power than the shaded cells resulting in curves (c) and (d) of Fig. 6. The cell of curve (b) in Fig. 6 has the highest probability of hot spot formation and is, therefore, the cell where the worst-case hot spot condition will occur.

F. Temperature Dependence Measurements

The effect of temperature on module performance parameters was investigated by heating the modules to a predetermined temperature ($\sim 80°C$) and then measuring the I-V characteristics as the modules are allowed to cool uniformly inside the simulator. These characteristics are then used to determine the dependence of I_{sc}, V_{oc}, and P_{max} on temperature.

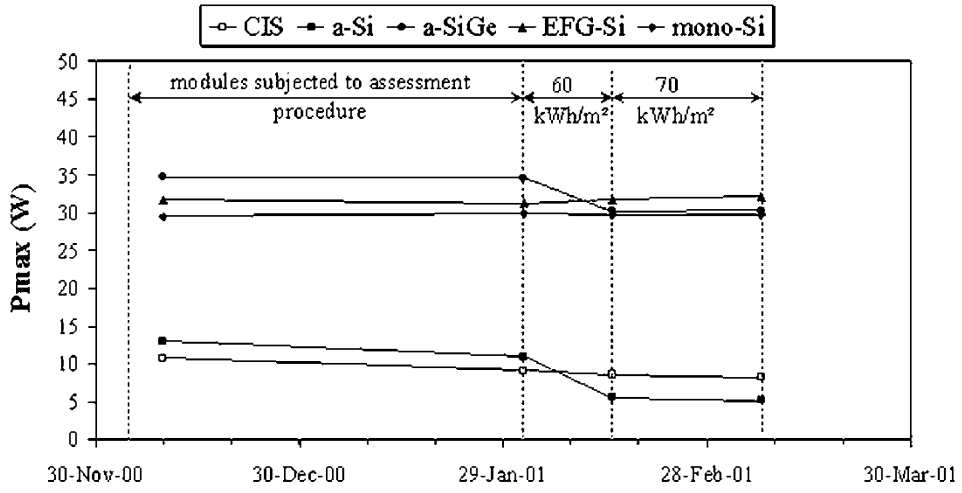

Fig. 10. Maximum power of the five modules at different times during the test period.

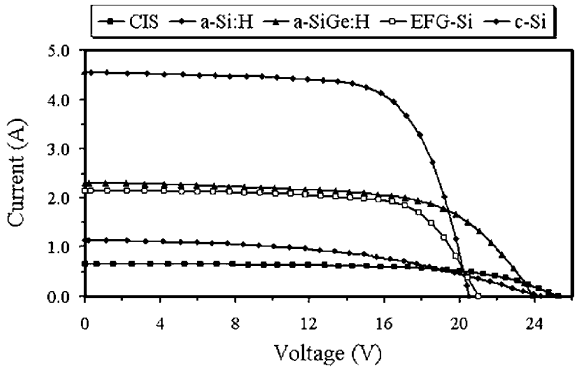

Fig. 11. I-V characteristics of the CIS, a-Si, a-SiGe, EFG-Si and mono-Si modules.

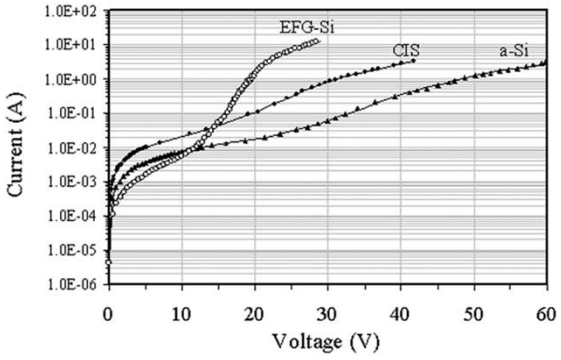

Fig. 12. Dark I-V charcteristics of the EFG-Si, CIS and a-Si modules.

G. Outdoor Monitoring

Most degradation modes result in a decrease in either the module's I_{sc} or V_{oc} or both. Therefore, by continuously monitoring these two parameters, degradation in module performance can immediately be observed. A system used to monitor the modules' I_{sc} & V_{oc} was designed and built at the University of Port Elizabeth and is illustrated in Fig. 7[14].

The data acquisition system (DAS) is PC based. HPVEE software is used to control instruments and acquire data every 10 minutes. When all relays are open, the modules' open-circuit voltages are measured. Relay 1 is then closed, and the first module's short-circuit current measured. Relay 1 is then opened, relay 2 is closed, and the second module's short-circuit current is measured. This process is repeated until I_{sc} for all modules has been measured. Data collected also includes module and ambient temperature, plane-of-array (POA) irradiance and wind speed at the modules.

IV. Experimental

Nine PV modules comprising different cell technologies were used in this study. For the purposes of this paper, only the results obtained from five of the modules representing different technologies are presented. The technology of the five modules, their specified and initial measured STC power, and their aperture area efficiency are listed in Table I. The assessment procedure discussed in Section IV is summarized in Table II. Also listed are the tests' objectives, and the frequency at which they are conducted.

All modules were initially subjected to the assessment procedure. The modules were then deployed outdoors on a fixed tilted, north facing rack. The modules' I_{sc} and V_{oc} were measured every 10 minutes. Light I-V characteristics were also measured at regular intervals. After the modules had been exposed to 130 sun-hours ($1\ \text{sun-hour} = 1\ \text{kWh/m}^2$) the modules were again subjected to the indoor assessment procedure. Results obtained before the modules were deployed outdoors, and after the 130 sun-hour exposure, are presented and discussed in the next section.

V. Results and Discussion

A. Visual Inspection and I-V Measurements

Figs. 8 and 9 show cracked cells in the EFG-Si and mono-Si modules, respectively. Also shown in these figures are the corresponding module I-V characteristics. The crack in the EFG-Si cell (Fig. 8(a)) runs across the cell, and the interconnect busbars are limiting the current loss. This is evident from the corresponding I-V characteristic Fig. 8(b), which has only a small indent in the upper current region. On the contrary, the crack in the mono-Si cell (Fig. 9(a)) runs alongside the interconnect busbar. This crack removes a part of the cell from its electrical circuit resulting in a relatively large mismatch in current produced. This is seen in Fig. 9(b), which has a bigger indent in the

TABLE III
ESTIMATED PARAMETERS AS OBTAINED FROM NON-LINEAR REGRESSION ANALYSIS OF MEASURED DATA.

Parameter	**CIS**	**a-Si**	**EFG-Si**
R_{sh}	10.35	48.07	88.11
I_{01}	4.93×10^{-508}	2.20×10^{-708}	3.57×10^{-322}
I_{02}	9.65×10^{-5}	1.56×10^{-6}	2.70×10^{-6}
n	2.35	5.29	1.63
R_s	3.64	6.83	0.83

upper current region as compared to Fig. 8(b). Figs. 8(b) and 9(b), therefore, clearly indicate how interconnect busbars can reduce power loss caused by cell breakage.

Fig. 10 shows the measured STC powers of all modules at different times during the test period. From this figure, it is evident that the CIS module gradually degraded with time. Both the a-Si and a-SiGe modules degraded significantly after the initial 60 sun-hour exposure. The two crystalline silicon modules showed no degradation during the test period. The performance of the CIS module degraded by 24% after being exposed to 130 sun-hours. The a-Si module degraded by about 60% after exposure. The dominant degradation mode in a-Si modules is the light-induced degradation as discussed earlier. The triple junction amorphous silicon (a-SiGe) module degraded by 13% after exposure. Fig. 10 illustrates the importance of light I-V measurements in identifying positively any degradation in module performance.

Fig. 11 shows the light I-V characteristics of the CIS, a-Si, a-SiGe, EFG-Si, and mono-Si modules after the 130 sun-hour exposure. The I-V curves show that there is a large variation in the FF, and hence, junction quality of the modules. The a-Si module had a FF of 31%, indicating that the quality of the cells is not very good. Since the FF is also a measure of the series resistance of the module, it is expected that the a-Si module will have a large series resistance. The FF of 74% for the EFG-Si module indicates a better junction quality and lower series resistance.

B. Dark I-V Measurements

Fig. 12 shows the dark I-V curves of the EFG-Si, CIS, and a-Si modules. The deviation of the curves from linearity in the high current range is due to the series resistance of a module, and in the low current range due to a leakage or shunt current. Using nonlinear regression analysis to fit the measured data to (2), estimated values for module shunt resistance (R_{sh}), series resistance (R_s), dark saturation current (I_0) and ideality factor (n) can be obtained. By periodically measuring the dark I-V characteristics of PV modules, changes in these parameters can be detected because the dark I-V characteristics are very sensitive to these parameters [8].

Table III lists the parameters obtained from nonlinear regression analysis of the measured dark I-V characteristics. The nonlinear fits all lie within a 99% confidence band and the standard deviations of all nonlinear fits from the measured data are less than 10^{-3} indicating that the estimated parameters obtained are in good accordance with the actual parameters. The shunt resistance and ideality factor values listed in Table III are average cell values.

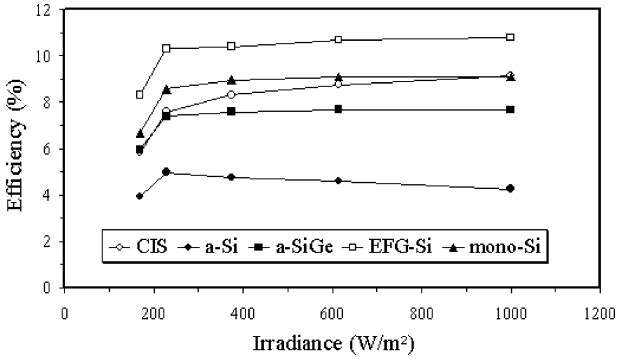

Fig. 13. Aperture area efficiency of the five modules as a function of light intensity.

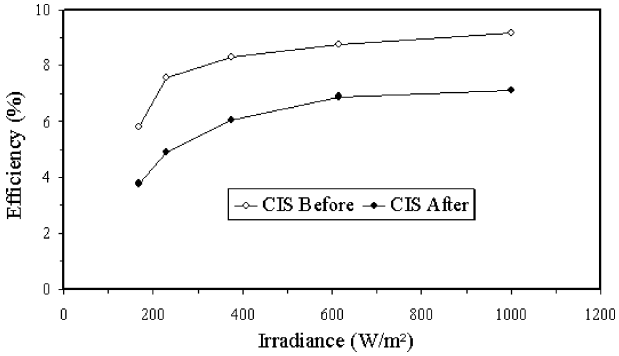

Fig. 14. Aperture area efficiency of the CIS module as a function of light intensity measured before and after the 300 sun-hour exposure.

C. Light Intensity and Individual Cell Shunt Resistance Measurements

The modules' behavior under various light intensities was first investigated. The aperture area efficiencies were measured as a function of light intensity. If the efficiency of a module first increases as light intensity is reduced, then the module is expected to have no cells with low shunt resistances. However, if the efficiency only decreases as light intensity is reduced, then the module is expected to have cells with low shunt resistance [11], [22]. Fig. 13 shows the aperture area efficiency of the five modules as a function of light intensity. It is evident from the figure that the CIS module exhibits shunting behavior because its efficiency only decreases as the light intensity is reduced.

These measurements were repeated after the modules have been exposed to 130 sun-hours. The efficiency of the CIS module is shown in Fig. 14 as a function of light intensity, as measured on 10 December 2000, and again after exposure.

The reduction of more than 20% in module efficiency is attributed to the gradual degradation as observed in Fig. 10, from

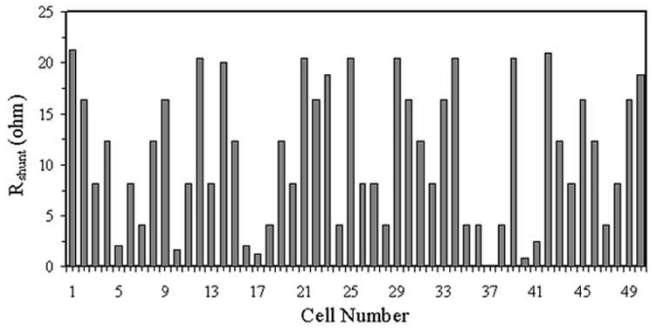

Fig. 15. Individual cell shunt resistance of the CIS module.

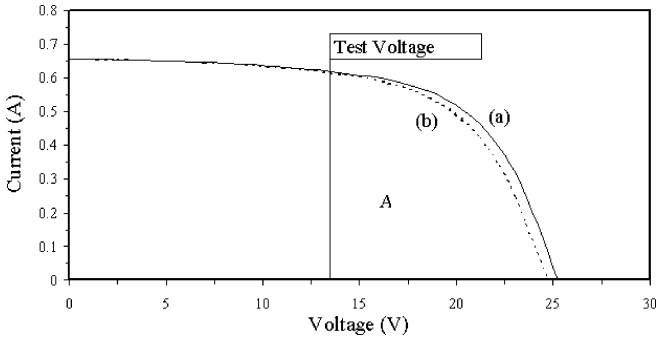

Fig. 16. I-V characteristics of the $CuInSe_2$ modules when fully illuminated (solid lines) and with one cell completely shaded (dashed lines).

10 December 2000 to 28 February 2001. Fig. 15 shows the individual cell shunt resistance of the CIS module. It is evident from this figure that the module has cells with low shunt resistances, which will detract from the module output, especially at low light intensities. The total module shunt resistance of 520 Ω is in excellent agreement with the 10.4 Ω/cell estimated from the dark I-V measurements for the 50-cell CIS module.

D. Worst-Case Cell Determination

The worst-case cell was determined for all the modules by sequentially darkening each cell and taking I-V curves. The shaded cell resulting in the highest module current at a predetermined test voltage is the cell where the worst-case hot-spot condition will occur. Fig. 16 shows the light I-V characteristics of the CIS module when (a) the module is fully illuminated and (b) an individual cell is shaded. The fully illuminated module produces a current of 0.613 A at the 14 V test voltage. The shaded cell resulting in curve (b) allows a current of 0.600 A to flow at 14 V. When individually shaded, the cells of the CIS module allow, on average, a current close to that of the fully illuminated module to flow, as measured at a typical test voltage of 14 V. This is not ideal because the module may be damaged when partially shaded, especially when there are no bypass diodes in the interconnection circuit, as is the case for this module.

Fig. 17 shows a photograph of the formation of hot spots on the a-Si module when cells were sequentially shaded. The experiment was terminated when the hot spots were forming. It was noticed that the longer the partially shaded module was exposed to the simulator light, the bigger the area of the hot spot. Therefore, partial shading of this module may be detrimental to the operation of the module. Integrating bypass diodes across each cell will reduce the possibility of cell damage due to hot spot formation.

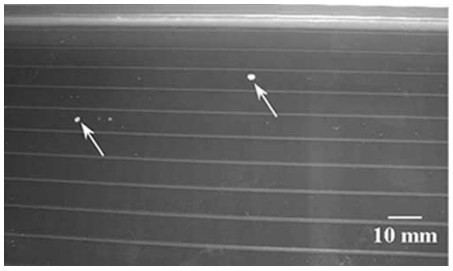

Fig. 17. Formation of hot spots on the a-Si module. The module was partially shaded and exposed to light in the simulator.

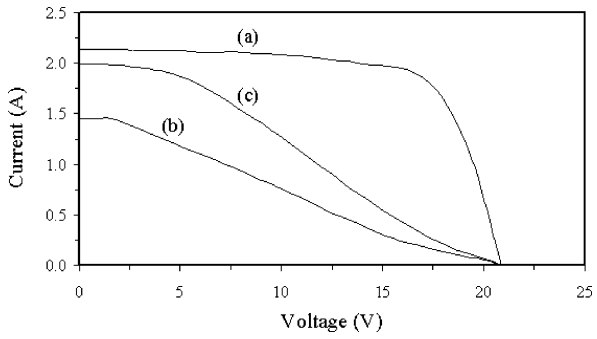

Fig. 18. Curve (a) is the fully illuminated module, (b) the module I-V curve when the cracked cell is fully shaded, and (c) module I-V curve when worst-case cell is fully shaded.

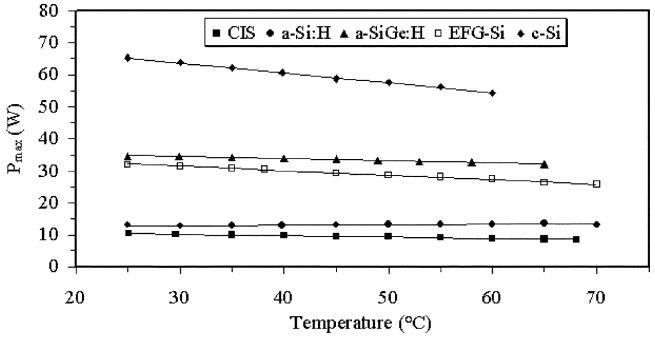

Fig. 19. Dependence of maximum power on temperature for all modules.

Fig. 18 shows the I-V curves of the EFG-Si module when (a) the module was fully illuminated, (b) the cracked cell in the module was fully shaded, and (c) the worst-case cell was fully shaded. The worst-case cell allows a relatively high current to flow through it, causing it to operate in the region of the breakdown voltage as was illustrated in Fig. 5. From Fig. 18, it is clear that the cracked cell is not the worst-case cell. The slopes of curves (b) and (c) between 15 and 20 V are measures of leakage currents. These currents stem from impurity centers in the semiconductor material [15]. The worst-case cell resulting in the highest current at the test voltage, when fully shaded, has the highest leakage current and hence, the lowest diode quality.

E. Determination of Temperature Coefficients

Fig. 19 shows the dependence of P_{max} on temperature for all modules. The slopes of these lines represent the temperature co-

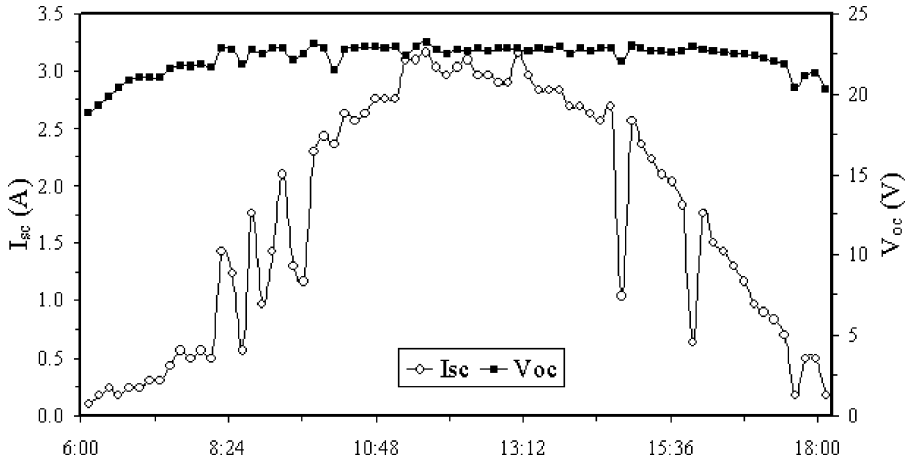

Fig. 20. $\mathrm{I_{Sc}}$ and $\mathrm{V_{Oc}}$ of the a-SiGe module measured on February 3, 2001.

TABLE IV
THE TEMPERATURE COEFFICIENTS FOR $\mathrm{I_{sc}}(\alpha)$, $\mathrm{V_{oc}}(\beta)$ AND $\mathrm{P_{MAX}}(\gamma)$ OF THE MODULES USED.

Module	CIS	a-Si:H	a-SiGe:H	EFG-Si	mc-Si	c-Si
α (mA/°C)	**0.06**	**2.70**	**1.20**	**1.70**	**0.90**	**2.10**
β (mV/°C)	**-96.0**	**-69.0**	**-73.1**	**-74.7**	**-81.4**	**-75.7**
γ (mW/°C)	**-41.7**	**-19.3**	**-65.3**	**-139.0**	**-147.0**	**-309.1**

efficient of maximum power, γ. From Fig. 19, it is evident that the modules' performances degrade with increases in temperature. Some modules, however, are more sensitive to temperature changes than others.

The temperature coefficients for $\mathrm{I_{sc}}(\alpha)$, $\mathrm{V_{oc}}(\beta)$ and $\mathrm{P_{max}}(\gamma)$ are listed in Table IV. The temperature coefficient for the short-circuit current is below $2\ \mathrm{mA/^{\circ}C}$ for all modules. The open-circuit voltage of the CIS modules, which is the highest at STC, is the most temperature dependent. The a-Si module's maximum power is the least temperature dependent of all modules. This is attributed to the lower junction quality of the a-Si module. The maximum powers of the crystalline modules with their higher quality cells are much more temperature sensitive than the thin-film modules.

F. Monitoring I_{sc} and V_{oc}

By monitoring a module's $\mathrm{I_{sc}}$ and $\mathrm{V_{oc}}$ continuously, it is possible to immediately detect any degradation in module performance. Fig. 20 shows the $\mathrm{I_{sc}}$ and $\mathrm{V_{oc}}$ of the a-SiGe module over one day, 3 February 2001. The variation in the short-circuit current is attributed to the variation in the plane-of-array (POA) irradiance because $\mathrm{I_{sc}}$ is directly proportional to incoming light intensity. The open-circuit voltage, however, depends logarithmically on light intensity [23]. Therefore, $\mathrm{V_{oc}}$ changes rapidly only if there is a large change in light intensity, as observed in the early morning and early evening. The relatively smaller variation in $\mathrm{V_{oc}}$ during the day is mainly due to temperature changes and cloud cover. By monitoring these two parameters continuously, module degradation or failure can be readily detected [14].

VI. SUMMARY AND CONCLUSIONS

This paper presents an assessment procedure used to evaluate photovoltaic (PV) modules. Results obtained from five PV modules employing different technologies were presented. Of these modules, the thin-film modules (Copper-Indium-Diselenide (CIS), single-junction (a-Si) and triple-junction (a-SiGe) amorphous silicon modules) showed degradation in performance after being deployed outdoors. The assessment procedure allows the determination of various module parameters including short-circuit current, open-circuit voltage, maximum power, fill factor, series resistance, shunt resistance, saturation current, ideality factor, the cell where the worst-case hot-spot condition will occur, and temperature coefficients. These parameters were then monitored at regular intervals to evaluate degradation.

Initial visual inspection revealed that the Edge-defined Film-fed Growth silicon (EFG-Si) and mono-crystalline silicon (mono-Si) modules had cracked cells. These cracks result in cell mismatch conditions. The mismatch in the EFG-Si module is limited by the interconnect busbar because the crack runs across the cell resulting in only a small loss in current collection capability.

After an initial exposure of 130 sun hours, the performance of the CIS module degraded by more than 20%. The a-Si module degraded by about 60%, and the a-SiGe module degraded by approximately 13%. The crystalline EFG-Si and mono-Si modules showed no degradation in performance. The cells in the CIS module had an average individual cell shunt resistance of about 10 Ω. If there are already shunt paths present across the junctions of cells in a module, light exposure may increase the number of shunt paths across the junction, reducing the module performance. The dominant performance degradation mode in the a-Si modules is light-induced degradation. By monitoring all module parameters with outdoor exposure, a qualitative as well as a quantitative assessment can be made on the reliability of PV module performance.

REFERENCES

[1] S. E. Forman, "Performance of experimental terrestrial photovoltaic modules," *IEEE Transactions on Reliability*, vol. R-31, pp. 235–245, 1982.

[2] L. N. Dumas and A. Shumka, "Photovoltaic module reliability improvement through application testing and failure analysis," *IEEE Trans. Reliability*, vol. R-31, pp. 228–234, 1982.

[3] J. A. Mazer, *Solar Cells: An Introduction to Crystalline Photovoltaic Technology*: Kluwer Academic Publishers, 1997, pp. 151–153.
[4] F. J. Pern and A. W. Czanderna, "EVA degradation mechanisms simulations those in PV modules," in *Proceedings of the AIP Conference*, 1992, p. 445.
[5] F. J. Pern, A. W. Czanderna, K. A. Emery, and R. G. Dhere, "Weather degradation of EVA encapsulant and the effect of its yellowing on solar cell efficiency," in *Proceedings of the 22nd IEEE PV Specialists Conference*, 1991, pp. 557–560.
[6] F. J. Pern, "Spectroscopic, scanning laser OBIC and $\mathrm{I\text{-}V}/\mathrm{QE}$ characterizations of browned EVA solar cells," in *Proceedings of the 25th IEEE PV Specialists Conference*, 1996, pp. 1255–1258.
[7] S. R. Wenham, M. A. Green, and M. E. Watt, *Applied Photovotlaics, Centre for Photovoltaic Devices and Systems*. Sydney: University of New South Wales, 1995, pp. 39–42.
[8] D. L. King and J. A. Hansen, "Dark current-voltage measurements on photovoltaic modules as a diagnostic or manufacturing tool," in *Proceedings of the 25th IEEE PV Specialists Conference*, 1997, pp. 1125–1128.
[9] *FitAll Nonlinear Regression Analysis: Research Edition*, MTR Software, 1998, pp. 130–141.
[10] S. R. Rummel and T. J. McMahon, "Effect of cell shunt resistance on module performance at reduced light levels," in *13th NREL Photovoltaics Program Review*, Lakewood, CO, 1995.
[11] E. L. Meyer, *Investigation of Properties and Energy Rating of Photovoltaic Modules, MSc-Dissertation*: University of Port Elizabeth, 1999, pp. 15–30.
[12] S. M. Sze, *Physics of Semiconductor Devices*: John Wiley and Sons, 1981, pp. 812–816.
[13] H. J. Möller, *Semiconductors for Solar Cells*: Artech House, 1993, pp. 41–46.
[14] E. L. Meyer and E. E. van Dyk, "Monitoring $\mathrm{I_{sc}}$, $\mathrm{V_{oc}}$ and performance parameters of photovoltaic modules," in *Proceedings of the 17th European Photovoltaic Solar Energy Conference*, 2001, pp. 524–527.
[15] W. Hermann, W. Wiesner, and W. Vaa en, "Hot spot investigations on PV modules-new concepts for test standard and consequences for module design with respect to bypass diodes," in *Proceedings of the 26th IEEE PV Specialists Conference*, 1997, pp. 1129–1132.
[16] D. L. Staebler and C. R. Wronski, "Reversible conductivity charges in discharge-produced amorphous Si," *Applied Physics Letters*, pp. 292–294, August 1977.
[17] J. Yang, A. Banerjee, T. Glatfelter, S. Sugiyama, and S. Guha, "Recent progress in amorphous silicon alloy leading to 13% stable cell efficiency," in *Proceedings of the 26th IEEE Photovoltaic Specialists Conference*, 1997, pp. 563–568.
[18] E. E. van Dyk, B. J. Scott, E. L. Meyer, and A. W. R. Leitch, "Temperature dependence of performance of crystalline silicon photovoltaic modules," *South African Journal of Science*, vol. 96, pp. 198–200, 2000.
[19] E. Lorenzo, *Solar Electricity: Engineering of Photovoltaic Systems*: PROGENSA, 1994, pp. 70–72. Translated by Philip Davies .
[20] T. J. McMahon, T. S. Basso, and S. R. Rummel, "Cell shunt resistance and photovoltaic module performance," in *Proceedings of the 25th IEEE PV Specialists Conference*, 1996, pp. 1291–1294.
[21] D. L. King, J. K. Dudley, and W. E. Boyson, "PVSIM: A simulation program for photovoltaic cells, modules and arrays," in *Proceedings of the 25th IEEE PV Specialists Conference*, 1996, pp. 1295–1297.
[22] E. L. Meyer and E. E. van Dyk, "Degradation analysis of silicon photovoltaic modules," in *Proceedings of the 16th European PV Solar Energy Conference*, 2000, pp. 2272–2275.
[23] E. E. van Dyk, E. L. Meyer, F. J. Vorster, and A. W. R. Leitch, "Long-term monitoring of photovoltaic devices," *Renewable Energy*, vol. 25, pp. 183–197, 2002.

Edson L. Meyer completed his PhD in Physics from the University of Port Elizabeth, South Africa, in 2001. His doctoral studies were on the reliability, degradation and failure of crystalline and thin-film modules. He is currently at the University of Fort Hare where he is heading the physics department. He is also managing research projects in (1) renewable energy and (2) construction science and architecture.

E. Ernest van Dyk received his PhD in Physics from the University of Port Elizabeth, South Africa, in 1994. He is currently at the University of Port Elizabeth and has spent one-year sabbaticals at the National Renewable Energy Laboratory, USA and at North Carolina State University. His research interests are photovoltaic module characterization and solar cell materials defect characterization.